Progress In Electromagnetics Research M, Vol. 108, 17–26, 2022

A Parametric Analysis of Modified Complementary Split Ring Resonator Low-Pass Notch Filter Suitable for the Coexistence of 5.8 GHz DSRC and 5.9 GHz ITS Applications

Alessandro Cidronali, Giovanni Collodi, Stefano Maddio, Lorenzo Pagnini, Marco Passafiume, and Giuseppe Pelosi

Abstract—We present a parametric analysis for a compact notch filter based on meta-material elements, suitable for the mitigation of interferences occurring at 5.9 GHz and impacting a 5.8 GHz DSRC receiver. The filter adopts a defected ground plane structure, which is derived by the class of complementary split ring resonator (CSRR) structures and further developed to improve the selectivity. The designed filter preserves the 5.8 GHz DSRC signal and attenuates the 5.9 GHz ITS-G5 signal of more than 20 dB, thus suited to improve dynamic range of DSRC vehicular receivers. This work introduces the new filter structure characteristics, its design principles, and the corresponding experimental validation.

1. INTRODUCTION

In the USA and EU (EC Decision 2008/671/EC), the Cooperative — Intelligent Transport Systems (ITS-G5) applications are allocated in the frequency bandwidth 5.850–5.925 GHz. They enable vehicle to vehicle (V2V) and vehicle to infrastructures (V2I) communications, aimed at improving safety and traffic management. In addition, to expedite the availability of Cooperative-V2X (C-V2X) services, the 5G Automotive Association is requesting a waiver of the European Commission's rules to deploy C-V2X in the 5.905–5.925 GHz portion of the ITS band. As a consequence, many analysts agree that the deployment of V2X technology, either C-V2X by the LTE-V2X radio access technology or the IEEE 802.11p based radio, will roll out in the present decade.

Within this context, deployment into 5.9 GHz range affects the existing V2I services such as the widely spread EU vehicular Electronic Toll Collection (ETC) and access control applications. The latter relies on Road Side Units (RSUs) and On Board Units (OBUs), which communicate by using backscattering transponder principle and operate in the 5.8 GHz range, namely from 5.785 up to 5.815 GHz. Thus, the coexistence between EU-DSRC and ITS-G5 needs to be taken into account [1, 2].

There are two possible interference scenarios, which impact in different ways on EU-DSRC OBU and RSU receivers. The first one is related to the out of band unwanted ITS transmitter emissions that fall in the RSU receiver bandwidth thus reducing its effective sensitivity (requirement is below −105 dBm). The second effect is related to the OBU receiver, which operates on the principle of the triggered radio and that could wake-up under signaling of the ITS transmitter, thus reducing the battery life of the OBU.

This scenario motivates the adoption of the interferences mitigation techniques that can be either active or passive. While the first is very effective, but compatible with RSU [3], the use of a passive filters represents a viable and effective solution for OBU front-end. Unfortunately, a compact filter technology suitable for OBU and capable to guarantee the required selectivity is not available to date.

Received 13 December 2021, Accepted 20 January 2022, Scheduled 4 February 2022
* Corresponding author: Alessandro Cidronali (alessandro.cidronali@unifi.it).
The authors are with the Department of Information Engineering, University of Florence, Via di S. Marta, 3, 50139, Florence, Italy.

A mature filter technology suited for this purpose is bulk acoustic wave (BAW), which permits to implement band pass filters and duplexers capable to select and reject the proper radio spectra. Although they are very effective for the below 3 GHz applications, their adoption for vehicular applications is still very challenging. For a BAW filter to work at 6 GHz, all the thin films in the layer stack — including the electrodes — must be very thin. Challenges arise regarding the electrical sheet resistance of the electrodes and the ability to create sufficiently smooth, uniform layers. Furthermore, the acoustic losses in solid materials tend to increase with the square of frequency. Specialized manufacturing processes are required to compensate temperature-related frequency drift and to ensure the required reliability.

More recently, a new technology enabling high performance microwave filters is based on defected ground structure (DGS) resonators, which are typically etched with various shapes and capable to properly interact with ground plane current flows [4]. From a behavioral point of view, DGSs act as parallel L-C resonators which resonate at given frequencies, depending on the their dimensions and shapes. Several applications demonstrate the potentiality of this structure as passband and stopband (notch) filter [5].

In this work we investigate the design principle for a notch filter designed to mitigate the above described interference issues and thus preserving the communication in the EU-DSRC frequency band while rejecting the power spectrum of the ITS emissions.

The filter is based on a modified version of the already introduced coplanar split-ring resonator (CSRR) technology [6, 7], capable to exhibit a stopband at 5.9 GHz and a corner frequency at 5.8 GHz. The paper introduces a parametric analysis of the modified CSRR and provides its design guidelines. According to the latter, a filter prototype was designed, fabricated, and tested to experimentally validate the design approach.

2. MODIFIED CSRR UNIT CELL STRUCTURE

The response of a notch filter is basically provided by the combination of a low-pass filter transfer function with a high-pass one and can be effectively described by the

$$T(\omega) = A\frac{s^2 + \omega_n^2}{s^2 + s\dfrac{\omega_0}{Q} + \omega_0^2}, \tag{1}$$

where ω_n and ω_0 represent respectively the frequencies of the conjugate zeros and poles, while Q is the notch filter quality factor that is related to the filter rejection steepness. Observing the transfer functions in Fig. 1 we recognize that depending on the relative positions of ω_n and ω_0, and the filter assumes two characteristic behaviors. For $\omega_n > \omega_0$ the filter behaves as a *low-pass notch,* cf. Fig. 1(a), with the peak $T(\omega_{\max})$ occurring below ω_n, while it behaves as a *high-pass notch* when $\omega_n < \omega_0$, cf. Fig. 1(b), with the peak $T(\omega_{\max})$ occurring higher than ω_0. In the particular case of $\omega_n = \omega_0$, the two

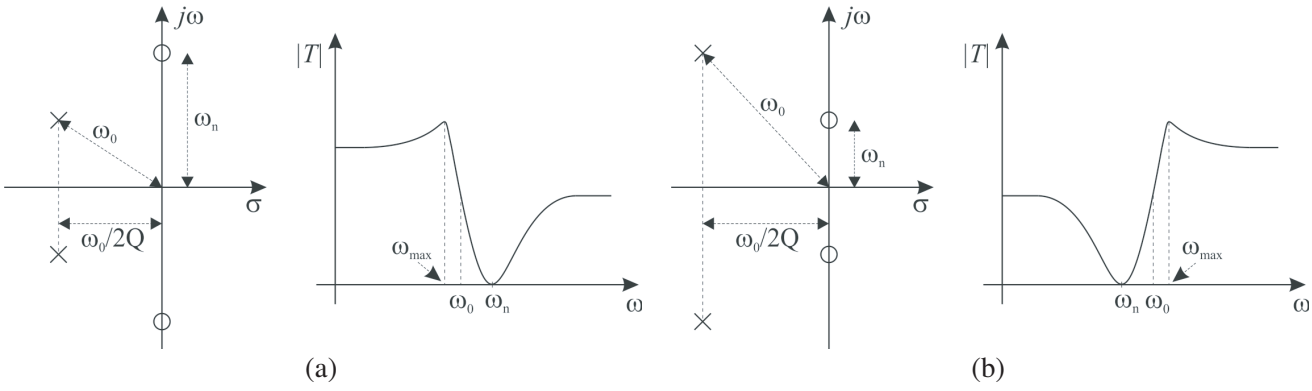

Figure 1. Second-order notch filters transfer functions, with respect to zero and pole mutual positions. (a) Low-pass notch. (b) High-pass notch.

versions of filters converge to the conventional notch filter having a symmetric transfer function about the notch frequency ω_n.

In the applicative scenario of interest, the EU-DSRC receivers operate with signals in the 5.795–5.815 GHz band, and the harmful frequency range extends from 5.875 to 5.925 GHz. In this context, the transition between the pass and stop bands is compatible with the low-pass notch version, while it appears impaired by the use of the high-pass notch configuration. For this purpose, we consider low-pass high-Q notch filter response centered at $\omega_n/2\pi = 5.9$ GHz, and in order to minimize the transition frequency bandwidth, thus maximizing the slope, we consider the implementation of a metamaterial unit cell implemented by a DGS [8, 9].

The core element of a DGS is a resonant slot in the ground metal, whose dimensions determine resonance frequency and consequently the poles and zeros in the transfer function.

In this paper, we consider the resonant structures described in [7], referred to a complementary split ring resonator (CSRR) as shown in Fig. 2(a), for which semi-analytical models for the design of notch filter and bandpass filter already exist [5, 10]. Nevertheless, simulations of those structures carried out by using a commercial CAD exhibited a high-pass notch behavior and a transition bandwidth too large for the specific purpose of the targeted applications. For this purpose, this work introduces the new resonant structure shown in Fig. 2(b).

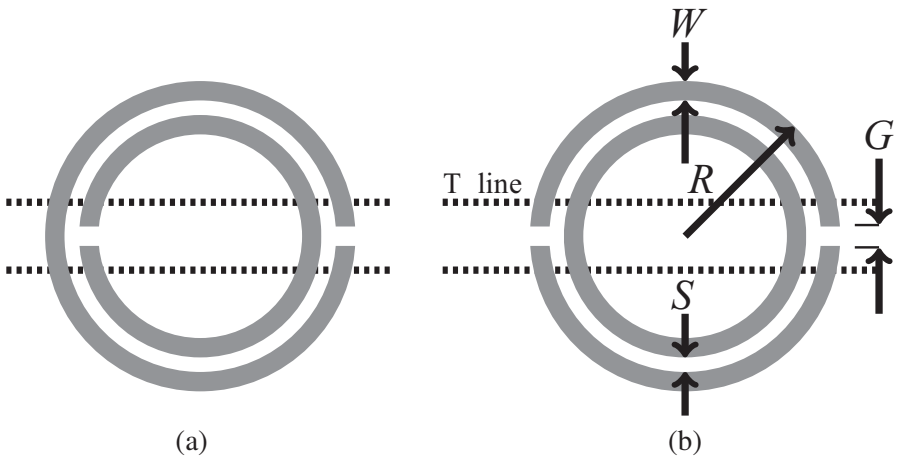

Figure 2. Comparison between complementary split ring resonator structures; dashed lines: microstrip transmission lines on upper layer. (a) CSRR. (b) Modified CSRR.

The equivalent circuit depicted in Fig. 3 is able to electrically reproduce the behavior of the proposed structure of Fig. 2(b) as well as the classic structure of Fig. 2(a). This is shown in Fig. 4, where the transmission parameter $|S_{21}|$ of the two structures obtained with electromagnetic simulations is compared with the one obtained from the equivalent circuit.

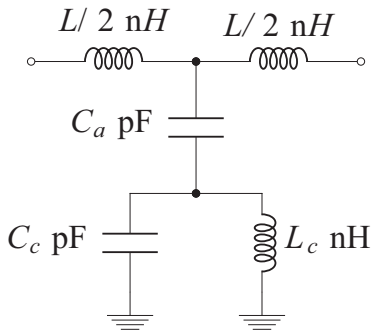

Figure 3. Electrical circuit model representing both the CSRR and the modified CSRR.

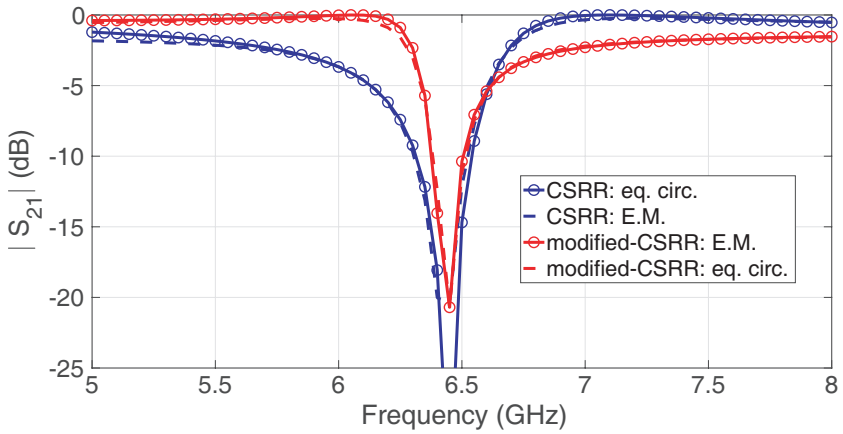

Figure 4. Comparison between CSRRs frequency response; the equivalent circuit models adopt to the following values. CSRR: $L = 0.049\,\text{nH}$, $C_a = 0.61\,\text{pF}$, $C_c = 3.11\,\text{pF}$, $L_c = 0.164\,\text{nH}$; modified-CSRR: $L = 0.977\,\text{nH}$, $C_a = 0.223\,\text{pF}$, $C_c = 1.367\,\text{pF}$, $L_c = 0.38\,\text{nH}$.

With respect to the classic CSRR the proposed geometry exhibits a comparable resonance frequency, with the same dimensions in terms of radius, R, space between conductors, S, and width W. In addition, it reflects an increase by a factor of 10 on the element L which, together with C_a, describes the coupling of the structure with the transmission line. These changes with respect to the conventional CSRR lead the structure to move from the high-pass notch behavior to the low-pass one, which is suitable for our purposes.

3. EQUIVALENT-CIRCUIT ANALYSIS

In this section, the analysis of the equivalent circuit of Fig. 3 is reported to justify the CAD-based simulations shown in Fig. 4.

Since in this context we are interested in the poles and zeros frequencies behaviors in dependence on the adopted structure, the idea is to derive ω_0 and ω_n as functions of the equivalent circuit elements.

For this purpose, we can proceed as follows. Since the equivalent circuit is a lossless network, it holds the well-known equation $S_{11}^2 + S_{21}^2 = 1$ from which we can observe that the maximum of S_{21} is reached when S_{11} is equal to zero, and vice versa. Thus, by setting S_{11} and S_{21} equal to zero and converting the S-parameters into Z-parameters, we obtain, respectively:

$$\frac{(Z_{11} - Z_0)(Z_{11} + Z_0) - Z_{12}^2}{Z_{11}^2 - Z_{12}^2} = 0 \tag{2}$$

$$\frac{2Z_0 Z_{12}}{Z_{11}^2 - Z_{12}^2} = 0 \tag{3}$$

and, by substituting in Eqs. (2) and (3) $Z_{11} = j\omega L/2$, $Z_{12} = \frac{1}{j\omega C_a} + \frac{1}{j\omega L_c + 1/j\omega C_c}$ and $Z_0 = 50\Omega$, we obtain for the four poles

$$\omega_{0_{1,2,3,4}} = \pm\sqrt{\frac{-\Lambda \pm \sqrt{\Lambda^2 - 4\Gamma\Sigma}}{2\Gamma}}, \tag{4}$$

and for the two zeros

$$\omega_{n_{1,2}} = \pm\frac{1}{\sqrt{L_c(C_a + C_c)}}, \tag{5}$$

where $\Gamma = C_a C_c L^2 L_c$, $\Lambda = 4C_a C_c L_c R_z^2 - C_a L^2 - 4C_a L L_c - 4C_c L L_c$ and $\Sigma = 4L - 4C_a R_z^2$.

Finally, by substituting in Eqs. (4) and (5) once the set corresponding to the CSRR structure, and then the one corresponding to the modified-CSRR structure, we obtain the expected behavior of

Table 1. Notch filter zeros and poles associated to the high-pass and low-pass behavior in Fig. 4.

	$\omega_0/2\pi$ (GHz)	$\omega_n/2\pi$ (GHz)
CSRR	7.07	6.44
modified-CSRR	5.78	6.47

high-pass notch and low-pass notch, respectively, as shown in Table 1. The data reported in Table 1 are the only meaningful ones.

4. PARAMETRIC ANALYSIS

Parametric simulations were carried out to determine the relations between the geometric parameters of the unit cell and the transition bandwidth.

Hereinafter, the stop frequency, f_{stop}, is defined where the transmission exhibits the maximum attenuation, while the pass frequency, f_{pass}, is defined as the frequency where the transmission drops of 1 dB with respect to the target pass-band. Finally, the transition bandwidth is assumed as the difference $f_{stop} - f_{pass}$. It is worth to mention that each of the described simulation is carried out by varying a geometric parameter while keeping the others constant in a range of values considered empirically suitable for the current analysis and realization feasibility.

Figure 5 reports the magnitude of the transfer parameter S_{21}, of the proposed filter, when the radius is varied from 3.5 mm to 3.95 mm. In response, the transmission parameter shifts almost rigidly. This response is even more evident in Fig. 6, where the f_{pass} and f_{stop} frequencies are fitted against R: in both cases the linear fitting reports almost the same slope. As a consequence, the transition bandwidth is constant with respect to the radius, R, which can be adopted to tune the notch filter in an effective way.

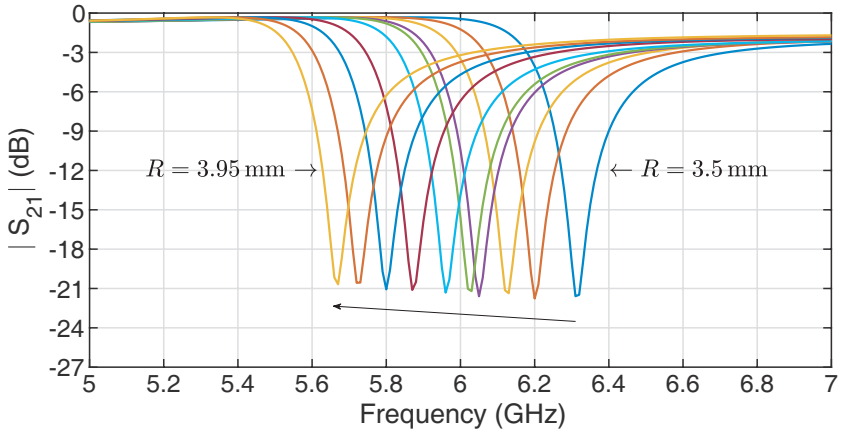

Figure 5. Transmission parameter of the filter as the radius R varies from 3.5 mm to 3.95 mm, step = 0.05 mm; $S = 0.20$ mm, $W = 0.53$ mm, $G = 0.33$ mm.

Figure 7 shows the transmission properties of the proposed filter when the inter-spacing, S, between the slots, is varied from 0.1 mm to 0.8 mm. In this case, both f_{pass} and f_{stop} decrease as S increases, but with different rates, thus resulting in the deformation of the shape of the transfer parameter response, across the parameter variation range. In Fig. 8, f_{pass} and f_{stop} are shown versus the variation of S. Again, a basic fitting is shown alongside the curves. It can be highlighted that the different slopes of the two features cause the broadening of the transition bandwidth, thus the parameter S should be kept as low as possible.

Figure 9 shows the last parametric analysis taken into consideration. When the modified CSRR slot width W increases from 0.1 mm to 0.9 mm, f_{pass} is almost constant, while f_{stop} increases, once

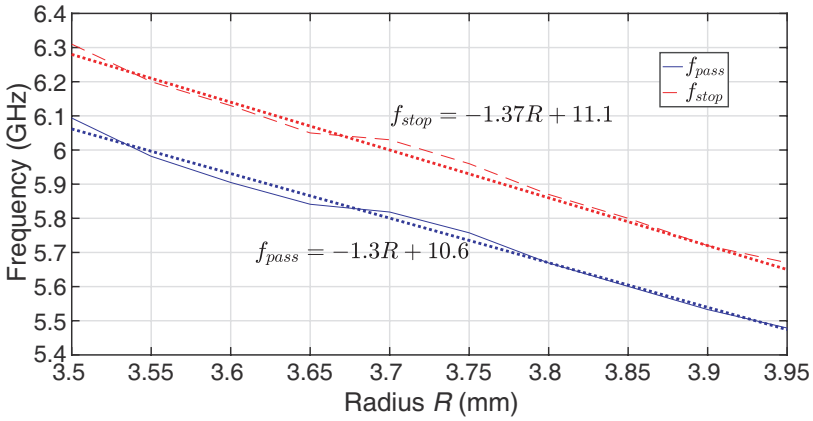

Figure 6. Variation of f_{pass} and f_{stop} for considered radius R values of Fig. 5.

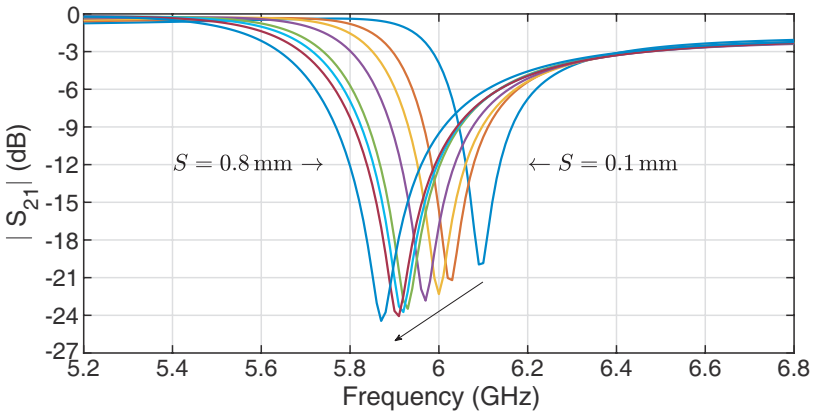

Figure 7. Filter transmission parameter as the inter-spacing S ranges from 0.1 mm to 0.8 mm, step = 0.1 mm; $R = 3.66$ mm, $W = 0.53$ mm, $G = 0.33$ mm.

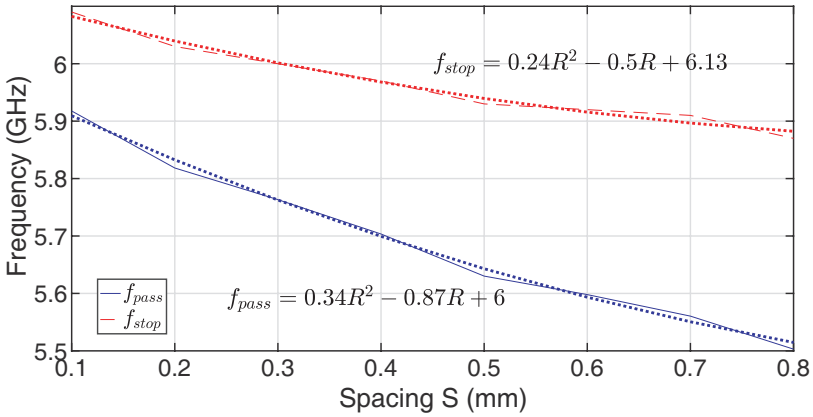

Figure 8. Variation of f_{pass} and f_{stop} for the considered range of the inter-spacing S. The polynomial fit is shown alongside the simulated traces.

again, almost linearly. In Fig. 10, f_{pass} and f_{stop} are shown versus W. From the graphs, it is evident that, also in this case, the transition bandwidth increases with the geometric parameter, thus also the parameter W should be taken at its minimum value.

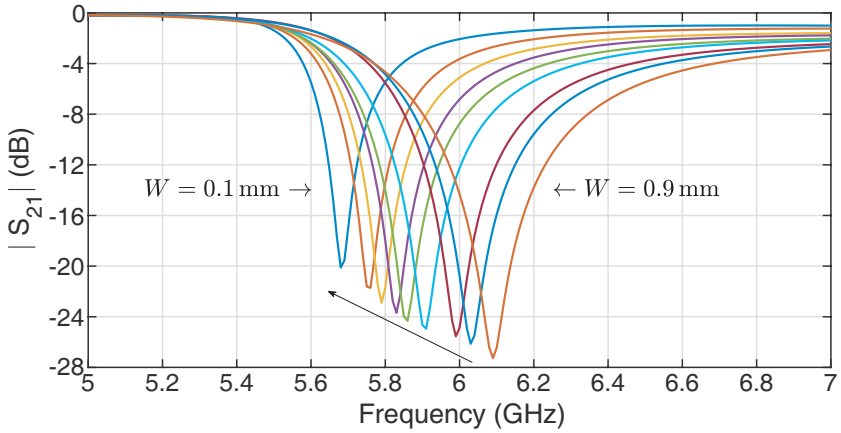

Figure 9. Transmission parameter of the filter as the slot width W varies from 0.1 mm to 0.9 mm, step = 0.1 mm; $R = 3.66$ mm, $S = 0.20$ mm, $G = 0.33$ mm.

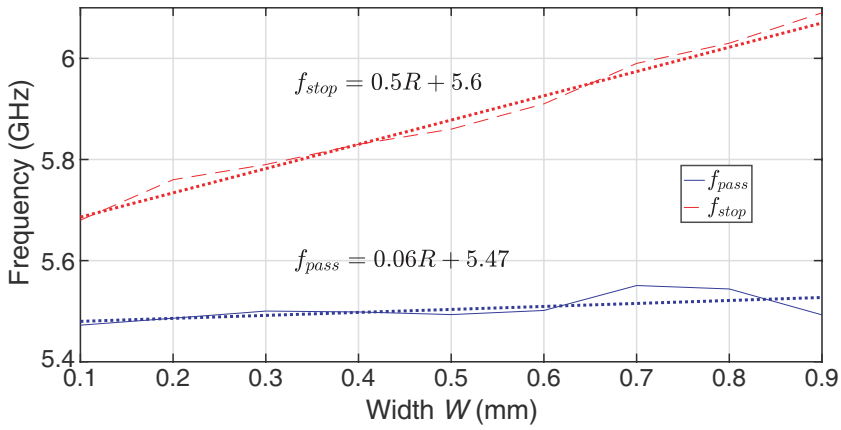

Figure 10. Variation of f_{pass} and f_{stop} for the considered range of slot width W of Fig. 9.

5. PROTOTYPE AND EXPERIMENTAL VALIDATION

For the specific application targeted by this work, a transition bandwidth of 100 MHz, i.e., $f_{pass} = 5.8$ GHz and $f_{stop} = 5.9$ GHz, is required. For this purpose, according to the parametric analysis, a filter composed of a single-cell would provide a transition bandwidth too large, thus a multi-cell structure is required. Nevertheless, the cascade of more unit cells introduces matching issues between unit cells, and thus an optimization procedure should be implemented in the design phase. Because the geometry of the structure is symmetric, we should expect that the impedances seen at the two cell ports is $Z_{in} = Z_{out}$. Therefore, impedance matching can be obtained simply adjusting distance between cells, that is the *p*eriod p of the structure. The optimization of a 4-cell cascade structure, within the design band specifications was carried out, considering the Taconic CER-10 laminate with thickness 25 mil, leading to the structure of Fig. 11. The optimized geometrical parameters are: $R = 3.66$ mm, $S = 0.2$ mm, $W = 0.53$ mm, $G = 0.33$ mm, $p = 7.55$ mm, while a picture of the filter prototype is shown in Fig. 12.

The design sensitivity to the geometrical parameters was analyzed by a Monte-Carlo simulation. For this purpose, the geometrical parameters were considered distributed uniformly within the interval defined by the optimized value $\pm 10\,\mu$m, with the latter assumed as the precision of the fabrication process. The results of the analysis are reported in Fig. 13 in terms of the transmission scattering parameter, along with the experimental data, in the frequency range $[5.6; 5.9]$ GHz. The simulated data

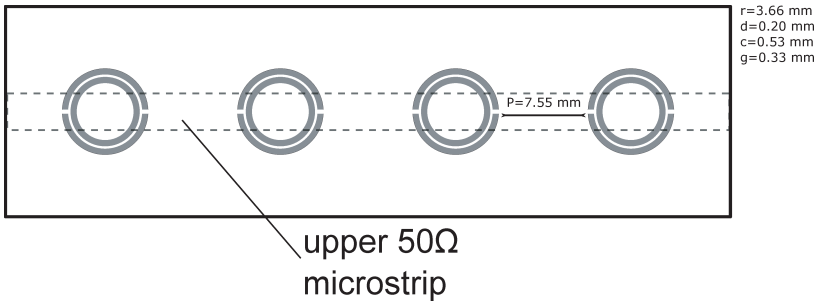

Figure 11. Layout of the implemented filter seen from the ground plane. The optimized design parameters value are: $R = 3.66\,\text{mm}$, $S = 0.2\,\text{mm}$, $W = 0.53\,\text{mm}$, $G = 0.33\,\text{mm}$, $p = 7.55\,\text{mm}$.

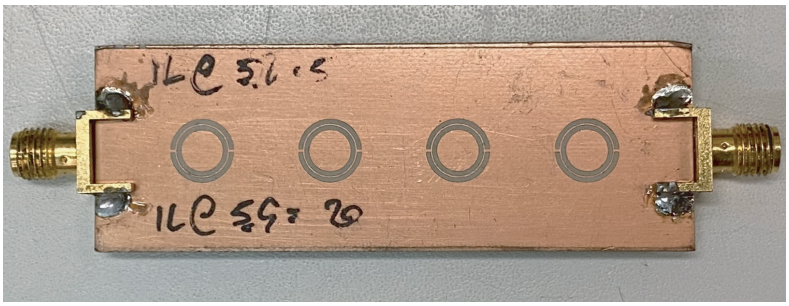

Figure 12. Picture of the implemented filter prototype seen from ground plane; the upper level contains the $50\,\Omega$ microstrip transmission line; fabricated on Taconic CER-10 laminate with thickness 25 mil, dimension of the modified-CSRR structure is $10 \times 66\,\text{mm}$.

are shown in terms of the mean value and the upper and lower limits evaluated at $\pm\sigma$. From the experimental data we estimate that the insertion loss at 5.8 GHz is 1.75 dB, while at 5.9 GHz it is in excess of 20 dB and keeps decreasing until it reaches the minimum of 37 dB at 5.975 GHz. The agreement between simulated $|S21|$ mean values and measurement within the transition bandwidth is observed, although simulations predict an average rejection in excess of 45 dB, and the measurement reaches a value in excess of 38 dB. It is worth nothing that this comparison is also affected by the measurement accuracy. In terms of sensitivity of the design, we observe that the slope of the transition bandwidth slightly increases moving from the *mean data* $-\sigma$ to *mean data* $+\sigma$.

Table 2. Comparison with state of the art notch filters operating in the 5.8 GHz frequency range.

	f_{pass} (GHz)	f_{stop} (GHz)	IL_{pass} (dB)	IL_{stop} (dB)	*slope* (dB/GHz)	Technology
[4]	5.80	6.10	−2.0	−15	43.3	DGS
[5]	5.80	6.10	−2.0	−20	60.0	CSRR
[6]	5.57	7.00	−1.8	−22	14.1	CSRR
[11]	5.80	6.00	−2.3	−12	48.5	CRLH
[12]	5.10	5.80	−5.5	−46	57.8	CSRR
[13]	6.10	6.20	−2.0	−8.0	60.0	SISLR
[14]	4.80	6.70	−2.0	−65	33.2	CRLH
This work	5.80	5.90	−1.7	−20	183.0	CSRR

CRLH: composite right/left-handed; DGS: transmission line defected ground structure; SISLR: stepped-impedance stub-loaded resonator; in [13] the design frequency is 5.8 GHz.

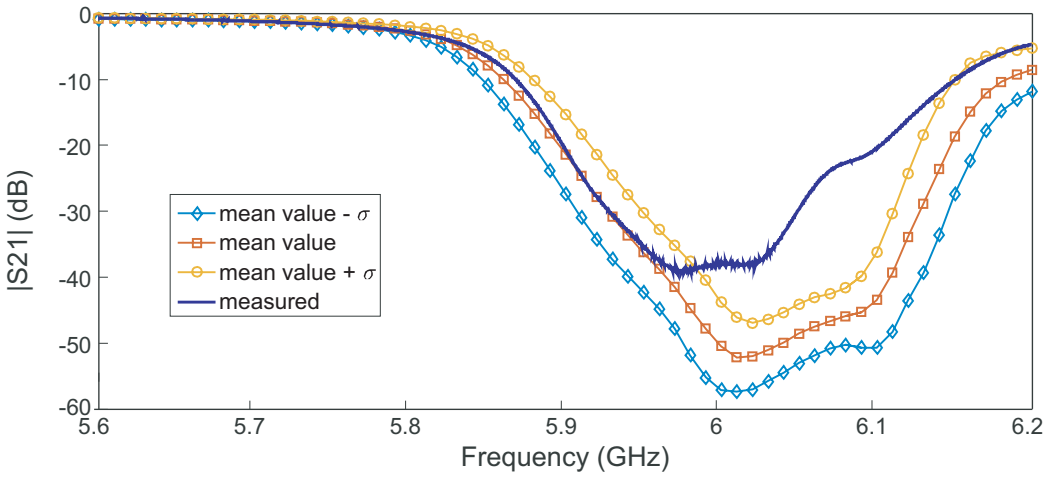

Figure 13. Comparison between statistical simulations and measurements results; all the device parameters are varied randomically with $\pm 10\,\mu$m with respect to their nominal value.

6. CONCLUSIONS

A modified CSRR based filter for the coexistence of 5.8 GHz and 5.9 GHz signals is proposed, analyzed with respect to its design parameters, fabricated, and validated. The resulting filter is compact and effective for on-board units of DSRC vehicular applications. It exhibits a reduced conversion loss of 1.75 dB at 5.8 GHz while attenuating the interference signal at 5.9 GHz in excess of 20 dB. For the sake of the comparison with the state of the art, Table 2 reports the experimental data associated with similar filter prototypes operating in the frequency band addressed by this work. The technologies taken into consideration, in addition to coplanar split-ring resonator [5, 6, 12], are the transmission line defected ground structure [4], stepped-impedance stub-loaded resonator [13], and composite right/left-handed [14]. The comparison is made in terms of the insertion loss (IL) exhibited at both the *pass-* and *stop-frequencies*, and specifically we calculated figure of merit *slope* $= 10^9|(IL_{pass} - IL_{stop})/(f_{pass} - f_{stop})|$. Adopting this figure of merit the prototype herein discussed exhibited a slope of 183 dB/GHz and remain the unique filter suitable to guarantee the coexistence between the EU-DSRC operating at 5.8 GHz and the ITS applications operating at 5.9 GHz.

The experimental validation demonstrates the effectiveness of the proposed device for the next development of for EU-DSRC OBU.

REFERENCES

1. Aigner, R., C. MacKenzie, and A. Zajac, "Advanced RF filters for V2V and other automotive applications," 2016 [Online], Qorvo Inc White Paper, url: https://www.qorvo.com/resources/d/advanced-rf-filters-for-v2v-and-automotive-white-paper.
2. Cidronali, A., S. Maddio, M. Passafiume, and G. Manes, "Car talk: Technologies for vehicle-to-roadside communications," *IEEE Microwave Magazine*, Vol. 17, No. 11, 40–60, 2016.
3. Maddio, S., A. Cidronali, and G. Manes, "Real-time adaptive transmitter leakage cancelling in 5.8 GHz full-duplex transceivers," *IEEE Transactions on Microwave Theory and Techniques*, Vol. 63, No. 2, 509–519, 2015.
4. Liu, J., W. Ding, J. Chen, and A. Zhang, "New ultra-wideband filter with sharp notched band using defected ground structure," *Progress In Electromagnetics Research Letters*, Vol. 83, 99–105, 2019.
5. Ghazali, A. N. and S. Pal, "UWB-BPF with application based triple notches and suppressed stopband," *Progress In Electromagnetics Research C*, Vol. 39, 149–163, 2013.

6. Soundarya, G. and N. Gunavathi, "Compact dual-band SIW bandpass filter using CSRR and DGS structure resonators," *Progress In Electromagnetics Research Letters*, Vol. 101, 79–87, 2021.
7. Baena, J. D., J. Bonache, F. Martín, R. M. Sillero, F. Falcone, T. Lopetegi, M. A. Laso, J. Garcia-Garcia, I. Gil, M. F. Portillo, et al., "Equivalent-circuit models for split-ring resonators and complementary split-ring resonators coupled to planar transmission lines," *IEEE Transactions on Microwave Theory and Techniques*, Vol. 53, No. 4, 1451–1461, 2005.
8. Breed, G., "An introduction to defected ground structures in microstrip circuits," *High Frequency Electronics*, Vol. 7, No. 11, 50–54, 2008.
9. Guha, D., S. Biswas, M. Biswas, J. Y. Siddiqui, and Y. M. Antar, "Concentric ring-shaped defected ground structures for microstrip applications," *IEEE Antennas and Wireless Propagation Letters*, Vol. 5, 402–405, 2006.
10. Bonache, J., I. Gil, J. Garcia-Garcia, and F. Martin, "Novel microstrip bandpass filters based on complementary split-ring resonators," *IEEE Transactions on Microwave Theory and Techniques*, Vol. 54, No. 1, 265–271, 2006.
11. Hu, S., Y. Gao, X. Zhang, and B. Zhou, "Design of a compact 5.7–5.9 GHz filter based on CRLH resonator units," *Progress In Electromagnetics Research Letters*, Vol. 89, 141–149, 2020.
12. Sassi, I., L. Talbi, and K. Hettak, "Compact multi-band filter based on multi-ring complementary split ring resonators," *Progress In Electromagnetics Research C*, Vol. 57, 127–135, 2015.
13. Mousavi, O., A. R. Eskandari, M. M. R. Kashani, and M. A. Shameli, "Compact UWB bandpass filter with two notched bands using SISLR and DMS structure," *Progress In Electromagnetics Research M*, Vol. 80, 193–201, 2019.
14. Shen, Y. Z. and C. L. Law, "5.8-GHz suppressed UWB bandpass filter EM-ploying modified CRLH-TL of two and three unit cell," *Progress In Electromagnetics Research Letters*, Vol. 29, 107–113, 2012.